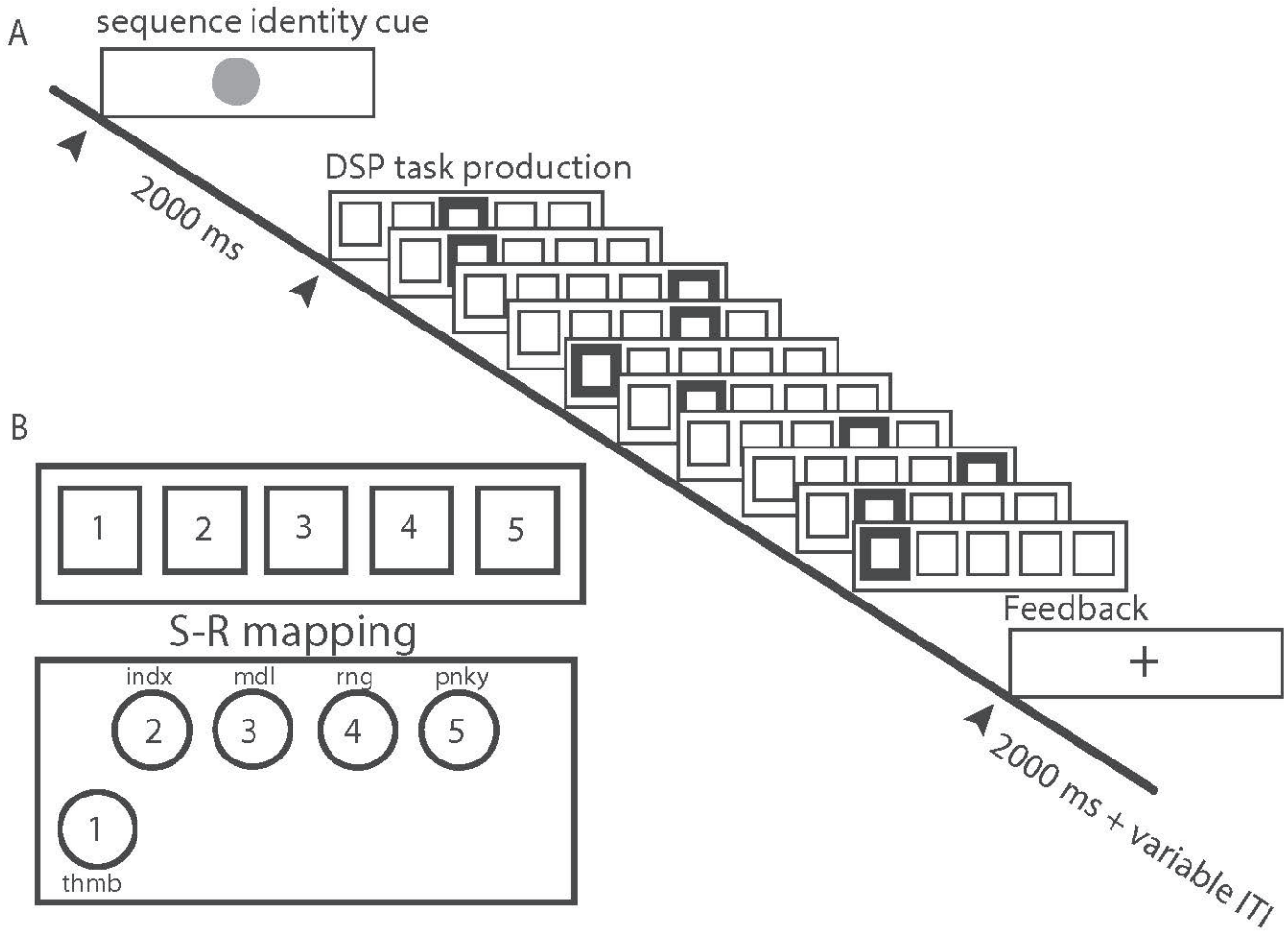

Supplementary Figure 1

Trial structure and stimulus-response (S-R) mapping.
(**a**) Each trial began with the presentation of a sequence-identity cue that remained on screen for 2 s. Each of the six trained sequences was paired with a unique identity cue. A discrete sequence-production (DSP) event structure was used to guide sequence production. The onset of the initial DSP stimulus (thick square, colored red in the task) served as the imperative to produce the sequence. A correct key press led to the immediate presentation of the next DSP stimulus (and so on) until the ten-element sequence was correctly executed. Participants received a '+' as feedback to signal that a sequence was completed and to wait (approximately 0–6 s) for the start of the next trial. This waiting period was called the 'intertrial interval' (ITI). At any point, if an incorrect key was hit, a participant would receive an error signal (not shown in the figure), and the DSP sequence would pause until the correct response was received. (**b**) There was direct S-R mapping between a conventional keyboard or an MRI-compatible button box (lower left) and a participant's right hand, so that the leftmost DSP stimulus cued the thumb and the rightmost stimulus cued the pinky finger. Note that the button location for the thumb was positioned to the lower left for maximum comfort and ease of motion.

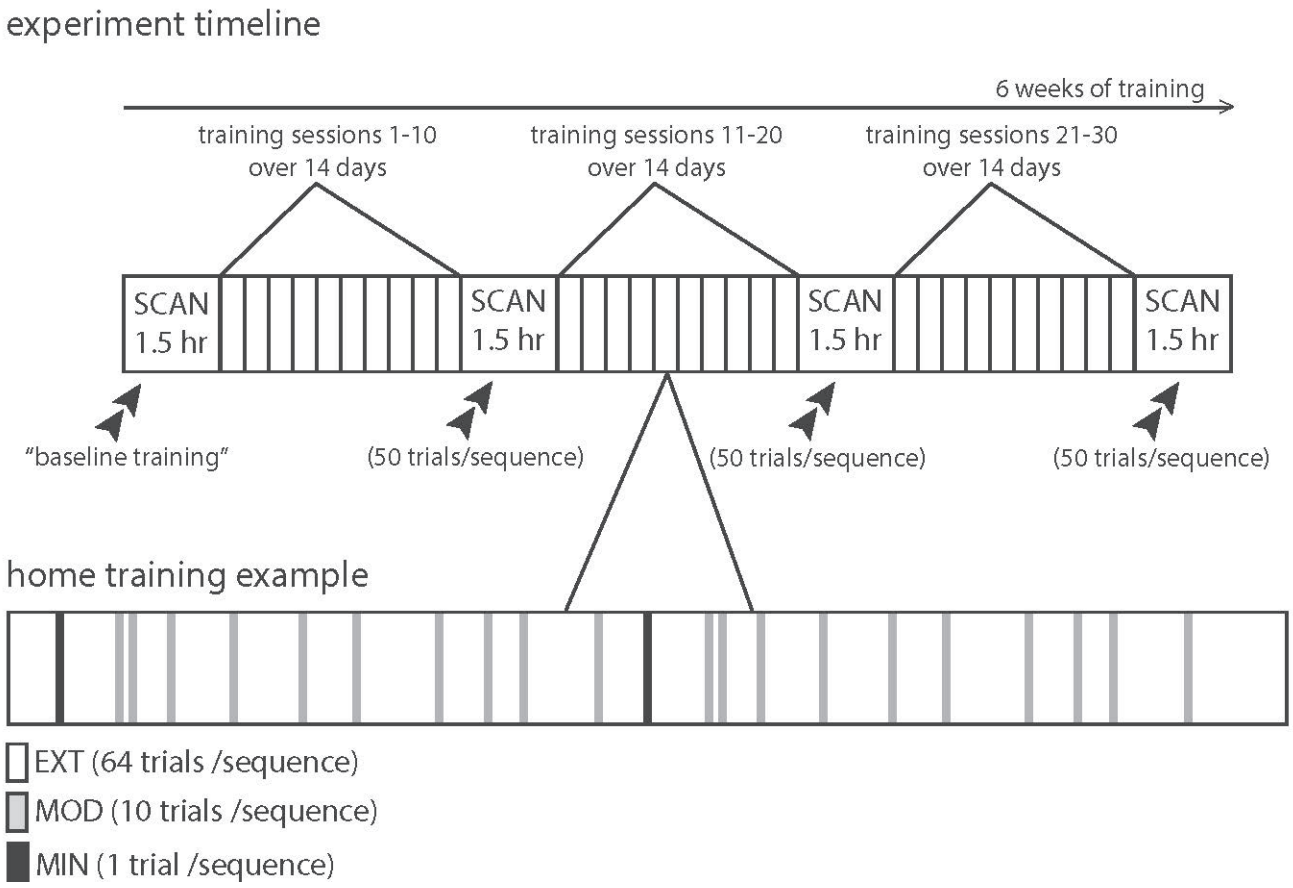

Supplementary Figure 2

Experiment timeline.

Training sessions in the MRI scanner during the collection of blood oxygen level–dependent (BOLD) signals were interleaved with training sessions at home. Participants first practiced the sequences in the MRI scanner during a baseline training session (top). After every approximately ten training sessions, participants returned for another scanning session. During each scanning session, a participant practiced each sequence for 50 trials. Participants trained at home between the scanning sessions (bottom). During each home training session, participants practiced the sequences in a random order. (We determined a random order using the Mersenne Twister algorithm of Nishimura and Matsumoto as implemented in the random-number generator rand.m of MATLAB version 7.1.) Each EXT sequence was practiced for 64 trials, each MOD sequence was practiced for 10 trials, and each MIN sequence was practiced for 1 trial.

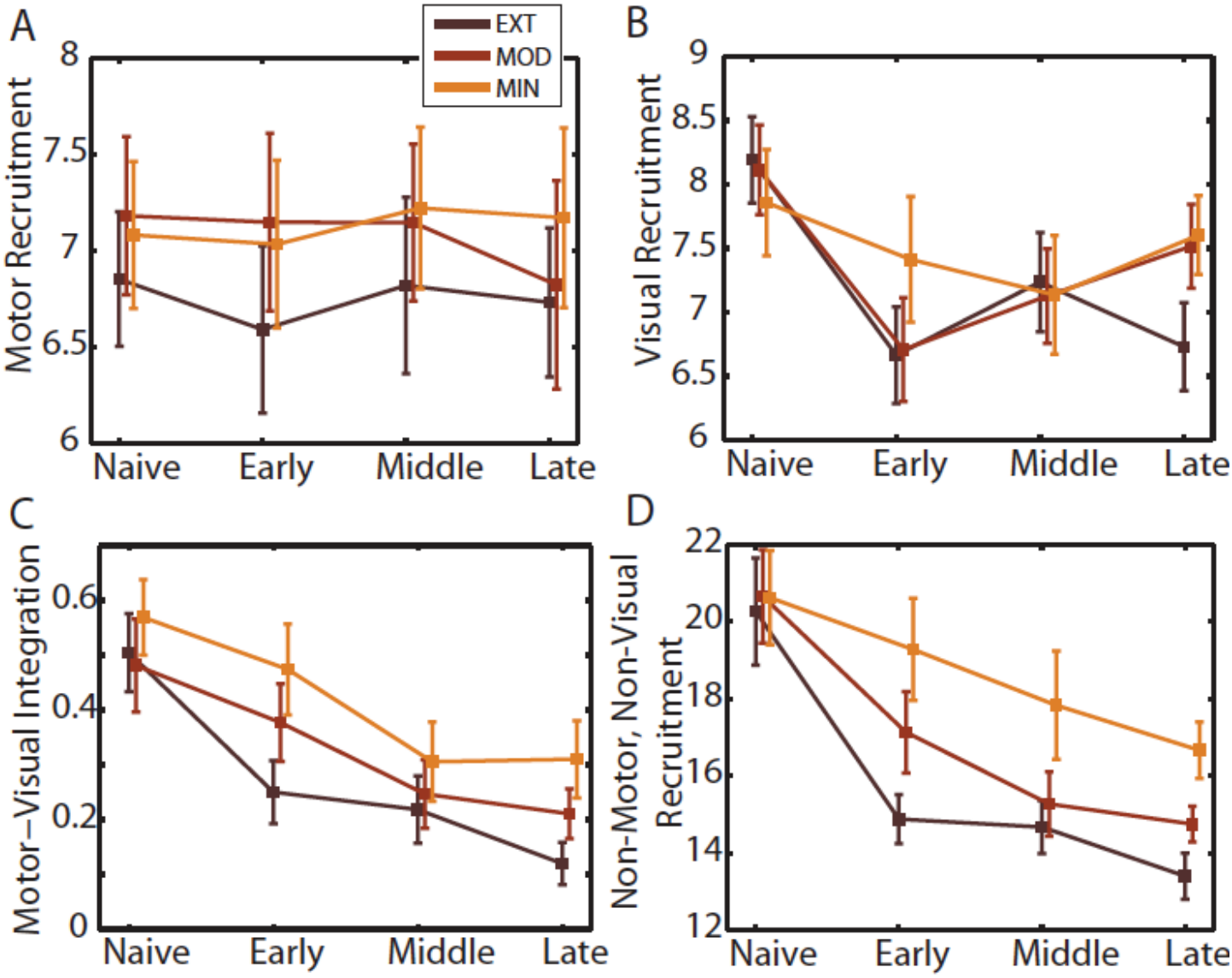

Supplementary Figure 3

Recruitment and integration are modulated by training, as shown by thresholded module-allegiance matrices.
In the article, we report the modulation of recruitment and integration by training, where 'training' is specifically measured by the number of trials practiced. In our experiment, we were able to obtain 12 different levels of training by using a combination of four different scanning sessions (each separated by approximately 2 weeks) and three different sequence types (extensive, EXT; moderate, MOD; and minimal, MIN). In the article, we show motor-visual integration and non-motor, non-visual recruitment as a function of the 12 training levels. For completeness, here we replot the same data with consideration of both scanning session and sequence type. Results shown in this figure were obtained using thresholded module-allegiance matrices, as opposed to those shown in **Supplementary Figure 4**, which were obtained using unthresholded module-allegiance matrices; the two figures show comparable results. (**a**) Motor and (**b**) visual recruitment was unaffected by training intensity (EXT (maroon), MOD (red), and MIN (orange) sequences) and duration (naive, early, middle, and late). (**c**) Integration between motor and visual modules and (**d**) recruitment of non-motor and non-visual cortices decreased with training intensity and duration. Error bars indicate s.d. of the mean across participants.

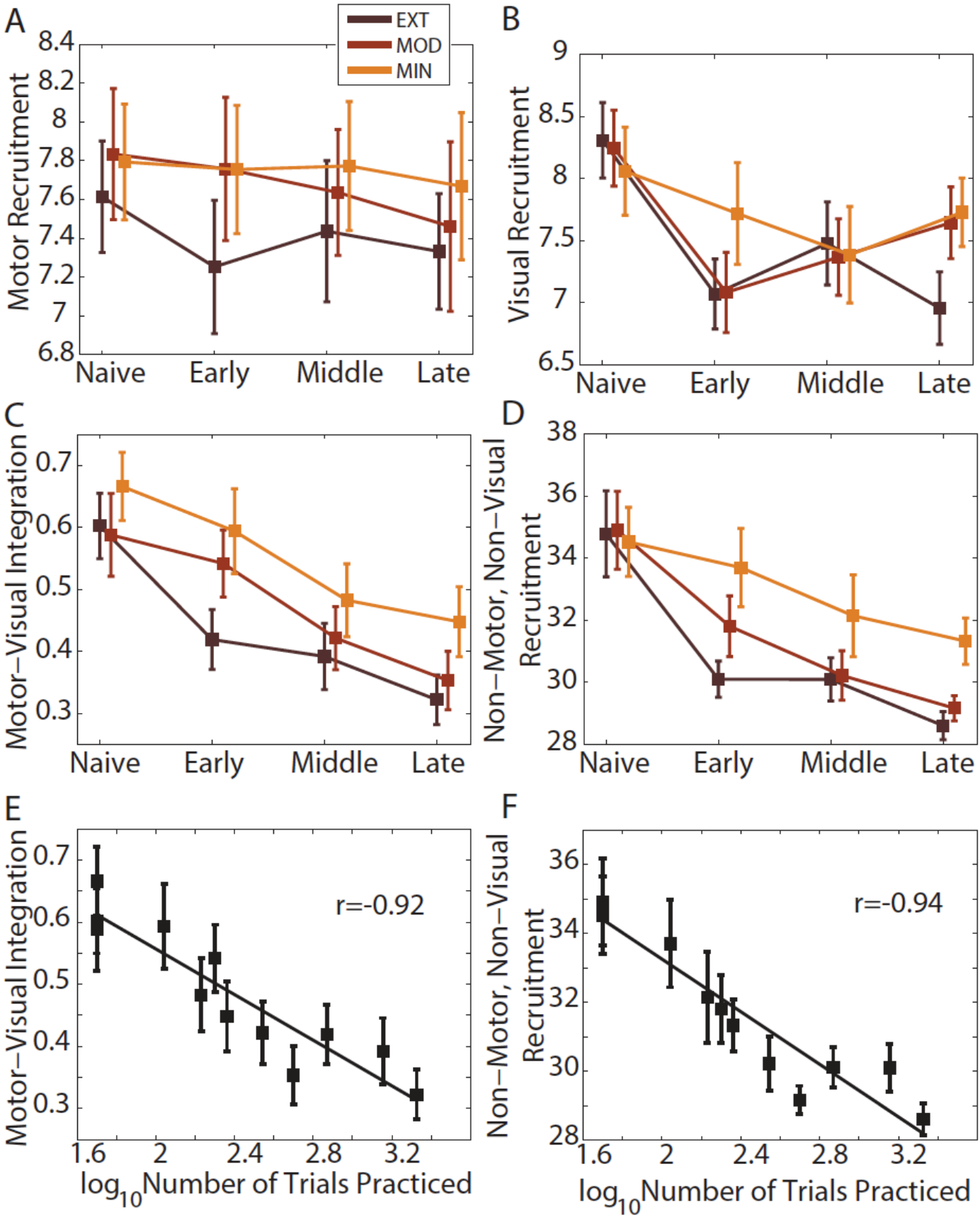

Nature Neuroscience: doi:10.1038/nn.3993

Supplementary Figure 4

Recruitment and integration are modulated by training, as shown by unthresholded module-allegiance matrices.
In the article, we use thresholded module-allegiance matrices to compute the recruitment and integration in the motor and visual modules and the non-motor, non-visual set, and to determine how these diagnostics are modulated by training. Here we demonstrate that these results are robust to the choice to statistically threshold the module-allegiance matrices. Results shown in this figure were obtained using unthresholded module-allegiance matrices and are comparable to those illustrated in **Figure 4** and **Supplementary Figure 3** (obtained using statistically thresholded module-allegiance matrices). (**a**) Motor and (**b**) visual recruitment was unaffected by training intensity (EXT (maroon), MOD (red), and MIN (orange) sequences) and duration (naive, early, middle, and late). (**c**) Integration between motor and visual modules and (**d**) recruitment of non-motor and non-visual cortices decreased with training intensity and duration. (**e**,**f**) The observations in **c** and **d** (i.e., that recruitment and integration depended on training intensity and duration) can be parsimoniously described by a single latent variable: the number of trials practiced (i.e., 'depth'). Solid diagonal lines indicate the best linear fit, and r values indicate Pearson correlation coefficients. The Pearson correlation coefficient for the data in **e** is $r = –0.92$, $P = 0.000022$, and for the data in **f** it is $r = –0.94$, $P = 0.0000055$. Error bars indicate s.d. of the mean across participants.

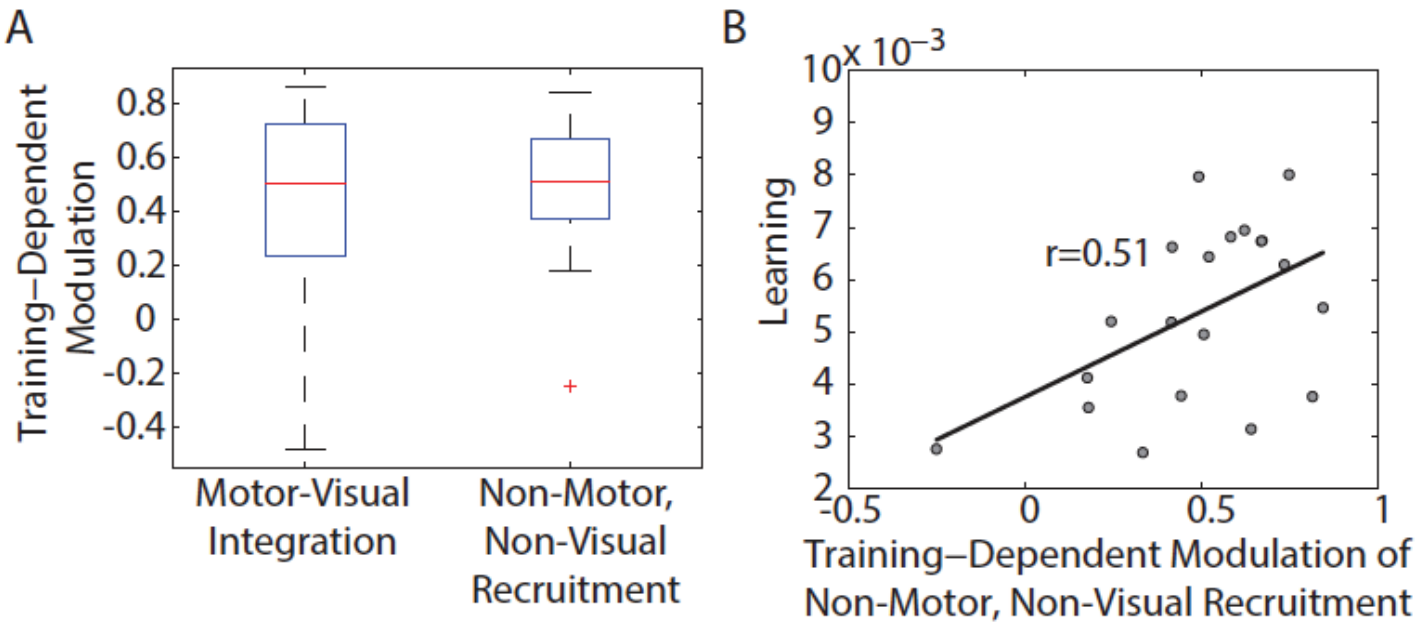

Supplementary Figure 5

Individual differences in brain network architecture map to task performance and task learning.
In the article, we use thresholded module-allegiance matrices to compute the recruitment and integration in the motor and visual modules and the non-motor, non-visual set, and to determine how these diagnostics are modulated by training. Here we show that these results are robust to the choice to statistically threshold the module-allegiance matrices. Results shown in this figure were obtained using unthresholded module-allegiance matrices and are comparable to those illustrated in **Figure 5** (obtained using statistically thresholded module-allegiance matrices). (**a**) Box plots of task-dependent modulation (correlation between network diagnostic and number of trials practiced) for both motor-visual integration (left) and non-motor, non-visual recruitment (right). (**b**) Scatter plot of learning rate and training-dependent modulation of non-motor, non-visual recruitment (Pearson's $r = 0.51$, $P = 0.021$).

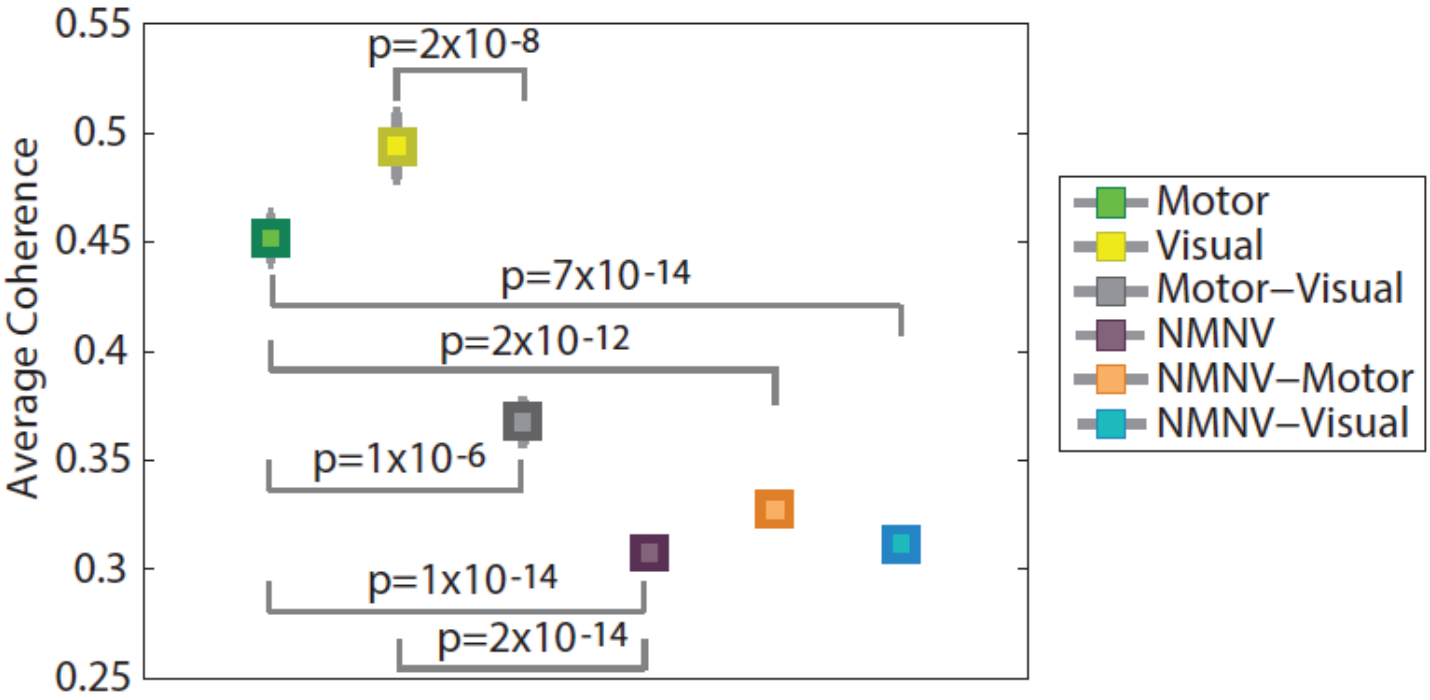

Supplementary Figure 6

Implications of module dissociation for time courses of BOLD activation.

In the article, we claim that (i) the dissociation of motor and visual modules indicates that brain areas in these two systems display significantly different time courses of BOLD activation, (ii) the non-motor, non-visual regions display significantly different time courses of BOLD activation than regions in the motor and visual systems, and (iii) the time courses of BOLD activation for regions of the non-motor, non-visual set differ significantly from one another. These claims are mathematically consistent with the formulation of the module-allegiance matrix and the utilization of the underlying community-detection approaches. In addition to these theoretical considerations, here we provide direct quantification of exactly how different the time courses of BOLD activation were in motor, visual, and non-motor, non-visual regions. In this figure, we show the average coherence between pairs of brain regions in which (i) both regions of the pair are within the motor module (green), (ii) both regions of the pair are within the visual module (yellow), (iii) both regions of the pair are within the non-motor, non-visual set (purple), (iv) one region of the pair lies in the motor module and the other region of the pair lies in the visual module (gray), (v) one region of the pair lies in the motor module and the other region of the pair lies in the non-motor, non-visual set (orange), and (vi) one region of the pair lies in the visual module and the other region of the pair lies in the non-motor, non-visual set (blue). These average values were computed per subject. *P* values for two-sided two-sample *t*-tests across subjects between these scenarios are given by the gray bars; note that all *P* values passed Bonferroni correction for multiple comparisons. Error bars indicate s.d. of the mean across participants.

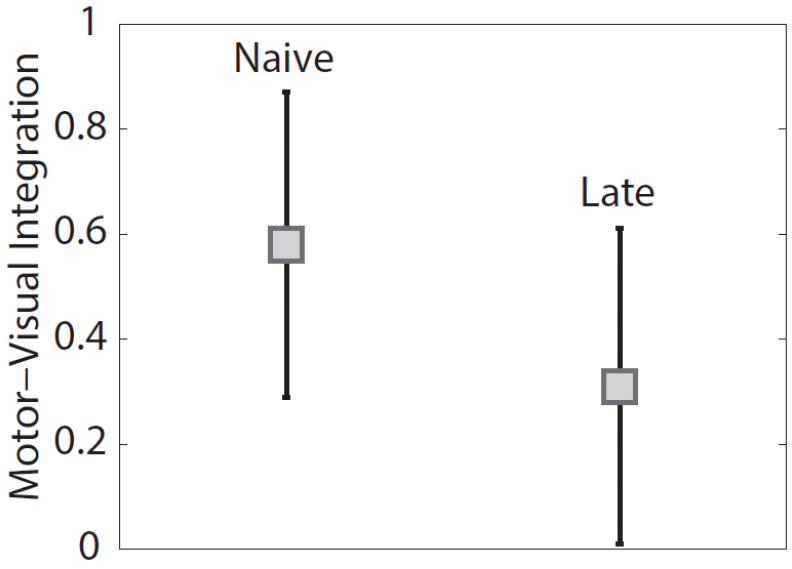

Supplementary Figure 7

Quantifying the change in sensorimotor autonomy induced by learning.

In the article, we describe data that support our conclusion that learning induces sensorimotor autonomy. In light of this conclusion, it is interesting to note that the motor and visual systems were quite pronounced as network communities even during early learning. Yet they were far from autonomous in the sense that regions of the two systems often tended to be present in the same network community or putative functional module. As learning progressed, the two systems became increasingly autonomous in the sense that the probability that regions of the two systems would be found in the same modules decreased significantly. To illustrate these points, we examined the motor-visual integration in the naive state (extensively practiced sequences in scan 1) compared to the motor-visual integration in the late-learning state (extensively practiced sequences in scan 4). The integration in the naive state (scan 1) was 0.58 (s.d. over subjects = 0.29), meaning that the probability that motor and visual modules would be in the same community in any given time window was greater than 50% (left; error bars indicate s.d.). In contrast, the integration in the late-learning state (scan 4) was 0.31 (s.d. over subjects = 0.30), meaning that the probability that motor and visual modules would be in the same community in any given time window was roughly 30% (right; error bars indicate s.d.). We observed that the two distributions of integration (in naive and late-learning states) were significantly different (two-sided two-sample *t*-test, $t = 2.92$, $P = 0.0058$), supporting our conclusion that learning induces relative autonomy of sensorimotor systems.

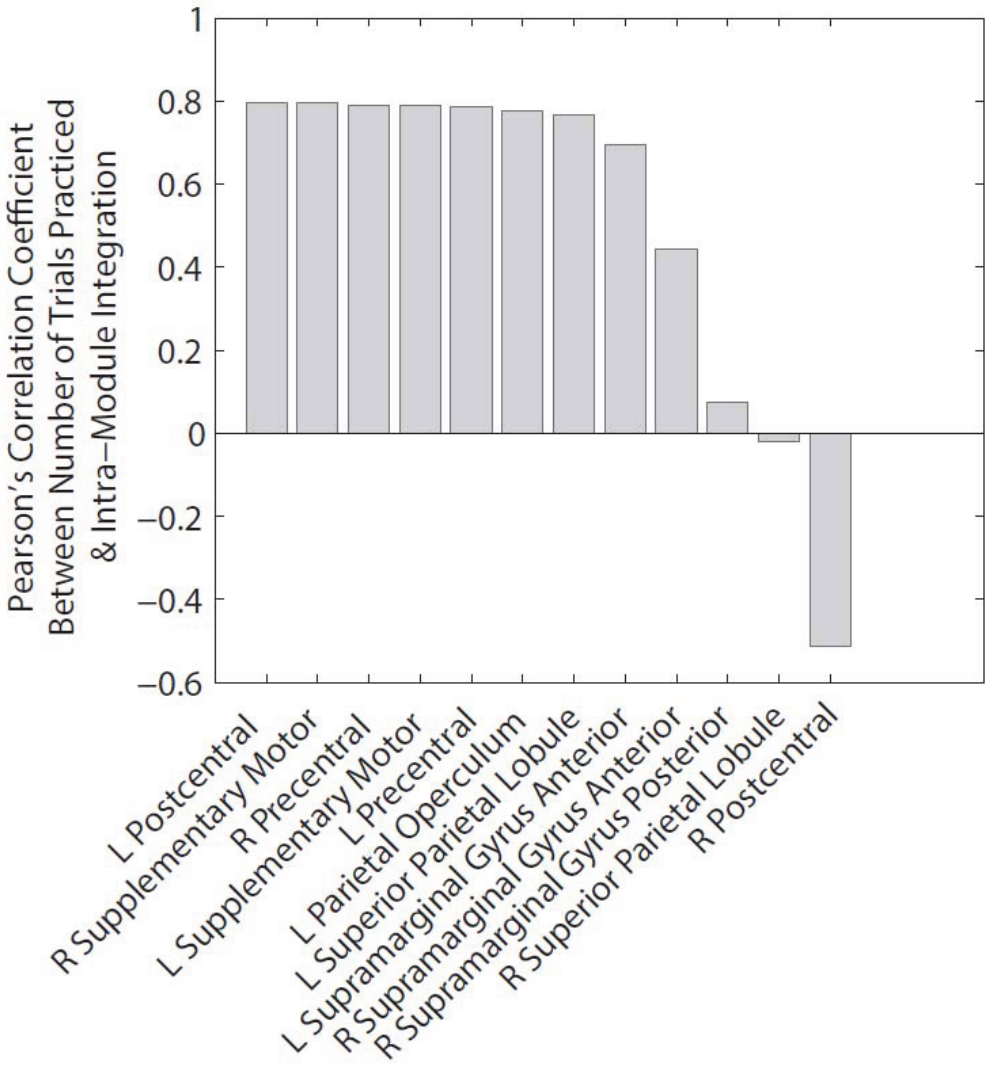

Supplementary Figure 8

Training-dependent modulation of intramodule integration for motor and visual systems.
Here we ask whether regions in the motor or visual systems integrate further or disengage from their respective modules with increasing task practice. Following the approach we used for the modules, we quantified, for each subject, the intramodule integration of a region with its own module as the sum of all functional connections between that region and other regions in its module. For example, the intramodule integration of the left SMA with the rest of the motor module is given by the sum over all j (not equal to i) in the motor module of P_{ij} for i = left SMA and j indexing the other 11 regions in the motor module. To determine whether this intramodule integration of a brain region increased or decreased with task practice, we calculated the training-dependent modulation of that region as –1 times the Pearson correlation coefficient between the group-averaged intramodule integration and the number of trials practiced. This figure shows the results for the motor module; 7 of the 12 regions showed significant disengagement from the motor module with training, as evidenced by associated P values that passed Bonferroni correction for 12 multiple comparisons: left SMA (r = 0.79, P = 0.0023), left precentral (r = 0.79, P = 0.0024), left postcentral (r = 0.80, P = 0.0019), left superior parietal (r = 0.77, P = 0.0036), right precentral (r = 0.79, P = 0.0023), right SMA (r = 0.80, P = 0.0020), and left parietal operculum (r = 0.78, P = 0.0030). No regions showed significantly enhanced integration with training. In the visual module, no regions showed significantly enhanced integration or disengagement with training.

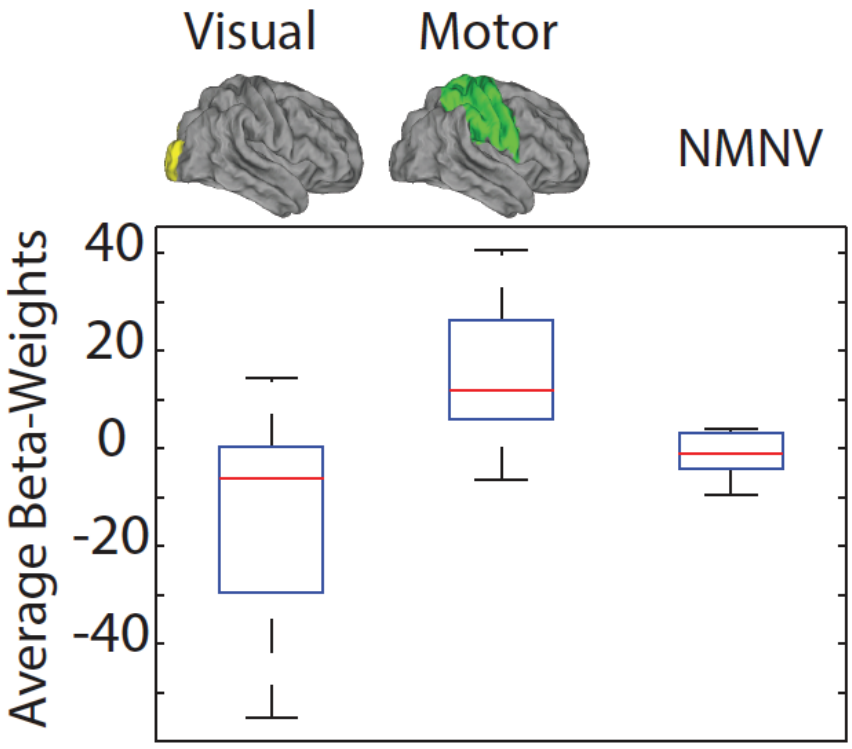

Supplementary Figure 9

Relationship between functional connectivity and activation.

The relationships between functional connectivity and functional activation during training are of critical interest. Here we ask whether the visual, motor, and non-motor, non-visual sets show different patterns of BOLD activation over the course of training. We performed a standard GLM analysis (see "Online Methods") to quantify the degree to which brain regions showed a linear decrease in activity over the course of training, and then we asked whether average beta weights of this GLM were different between functional modules. In this figure, we observe that the motor module showed predominantly positive beta weights (one-sided one-sample *t*-test showed that the mean was significantly greater than 0: $t = 3.01$, $P = 0.0071$), indicating a decrease in activation during learning. The visual module showed predominantly negative beta weights ($t = 5.14$, $P = 5.8 \times 10^{-5}$), indicating an increase in activation during learning. The non-motor, non-visual set of regions on average showed beta weights close to zero ($t = 1.27$, $P = 0.22$). Box plots indicate variation of the mean across participants. See "Online Methods" for a description of the GLM analysis used to estimate beta weights. It is interesting to compare these results to those obtained from functional connectivity measurements. Motor module: from the GLM analysis, we learned that the motor module showed a decrease in BOLD activation over the course of training; from the functional connectivity analysis, we learned that the motor module showed no change in network recruitment over the course of training (**Supplementary Fig. 3a**) but did show a decrease in integration with the visual module (**Supplementary Fig. 3c**). Visual module: from the GLM analysis, we learned that the visual module showed an increase in BOLD activation over the course of training; from the functional connectivity analysis, we learned that the visual module showed no change in network recruitment over the course of training (**Supplementary Fig. 3b**) but did show a decrease in integration with the motor module (**Supplementary Fig. 3c**). Non-motor, non-visual set: from the GLM analysis, we learned that the non-motor, non-visual set showed no change in BOLD activation over the course of training; from the functional connectivity analysis, we learned that the non-motor, non-visual set showed an exponential decrease in network recruitment over the course of training (**Supplementary Fig. 3d**). This pattern of results clearly shows that functional connectivity–based analyses provide complementary (and not redundant) information relative to activation-based analyses. In particular, the two features of learning-related changes in connectivity reported in the article—decreases in motor-visual integration and decreases in non-motor, non-visual recruitment—are not observable in activation-based analyses. Finally, the prediction of individual differences in learning on the basis of decreases in non-motor, non-visual recruitment could not be done using activation-based analyses in which non-motor, non-visual activity did not change as a function of training. These results highlight the utility of network-based approaches in uncovering previously hidden features of cognitive processes and individual variation in the performance of those processes.

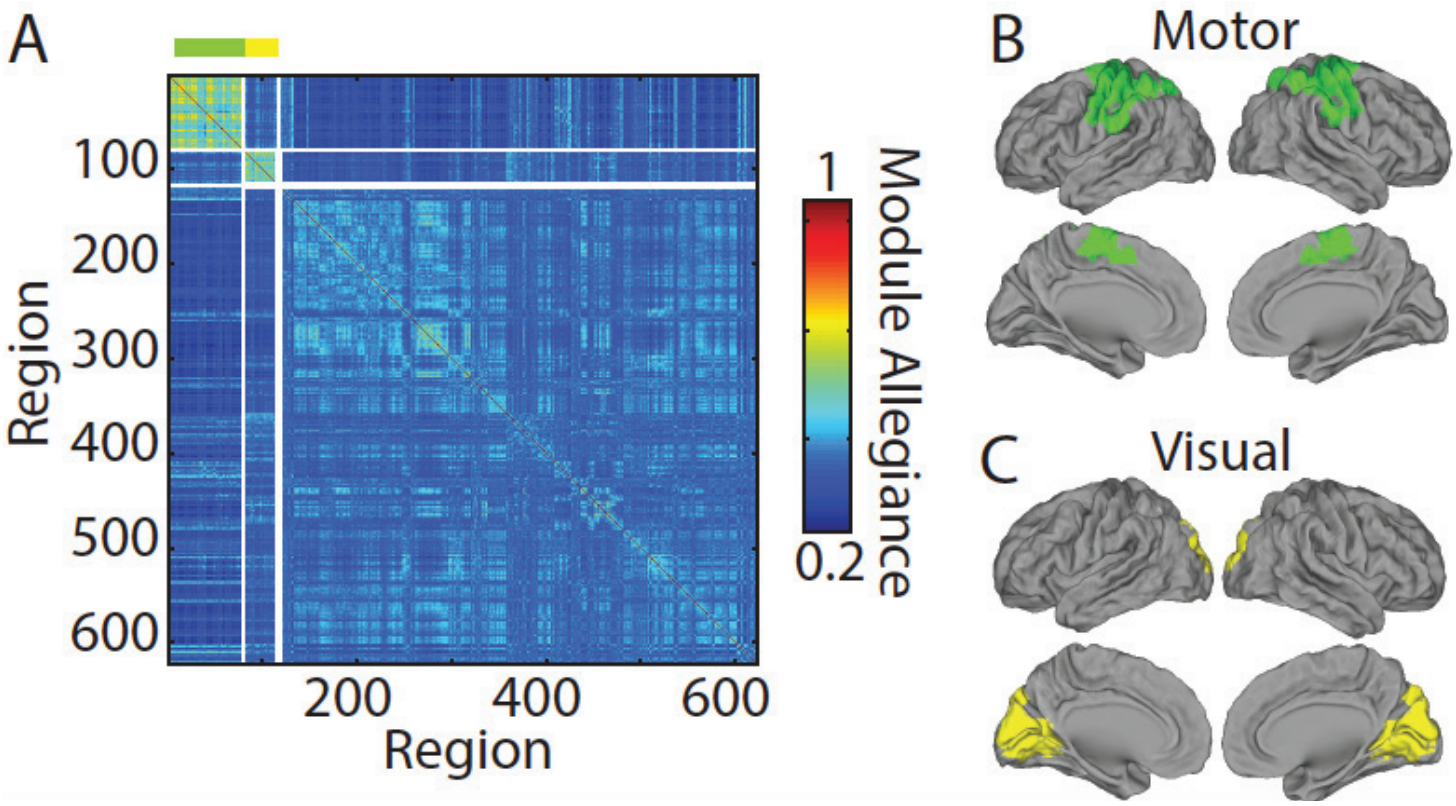

Supplementary Figure 10

Summary architecture of learning in finer-grained parcellation.
It was important to examine the robustness of our results to changes in the granularity of the whole-brain atlas used. In the next few supplementary figures, we report a reanalysis of our data with a new parcellation scheme composed of smaller regions of interest. We combined two separate atlases: (i) the AAL-derived 600-region atlas that we developed for use in refs. 68 and 69, which subdivides the 90 AAL anatomical regions into regions of roughly similar size via a spatial bisection method, and (ii) a high-resolution probabilistic 26-region atlas of the cerebellum in the anatomical space defined by the MNI152 template, obtained from T1-weighted MRI scans (1-mm isotropic resolution) of 20 healthy young participants[70,71] (this latter atlas is provided by SPM8). The combination of these two atlases provided a high-resolution, 626-region atlas of cortical, subcortical, and cerebellar regions. We called this new atlas the AAL-626 atlas. Following the same procedures outlined for the Harvard-Oxford atlas, we constructed a module-allegiance matrix and observed the presence of two strong modules, which corresponded to the motor and visual systems. (**a**) The module-allegiance matrix that indicates, for a pair of nodes, the probability that those two nodes will be located in the same functional community across subjects, scanning sessions, sequence types, and trial blocks. Similar to that reported in the article for the coarser-grained parcellation, this module-allegiance matrix displays two putative functional modules composed of brain regions that were consistently grouped into the same network community: (**b**) one composed of primary and secondary sensorimotor areas, and (**c**) one composed of primary visual cortex. Brain regions in **a** have been ordered to maximize strong associations along the diagonal.

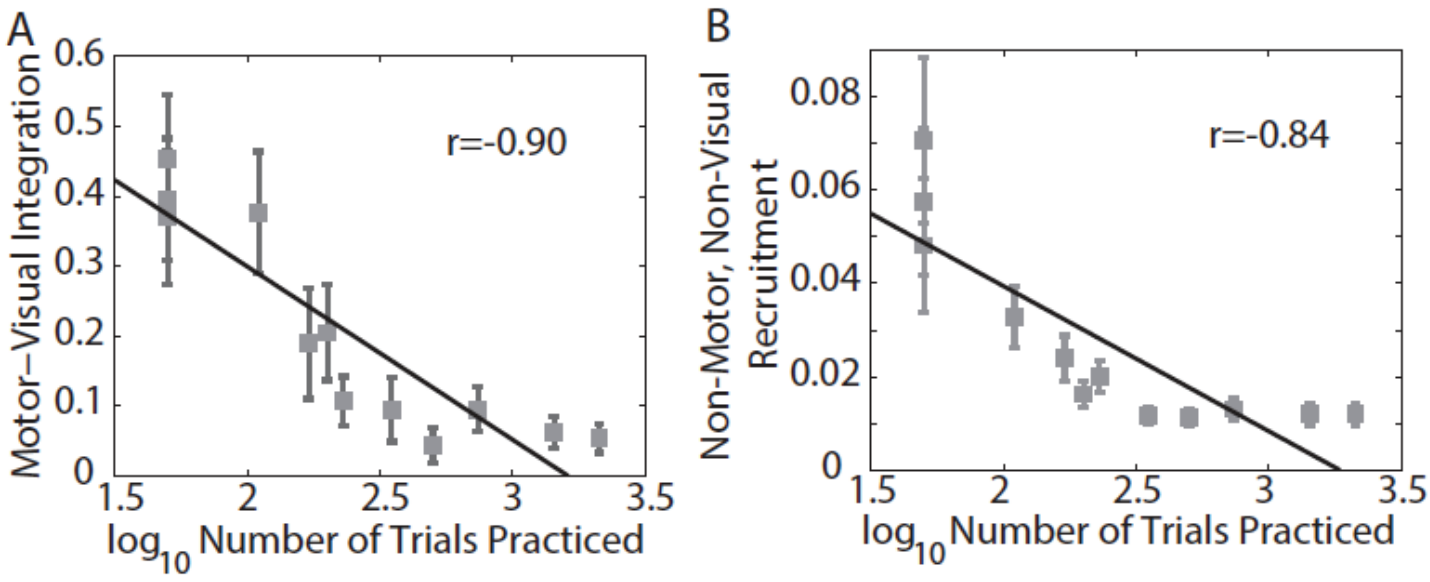

Supplementary Figure 11

Recruitment and integration modulated by training in finer-grained parcellation.
Consistent with results reported in the article, we observed that (i) motor-visual integration and (ii) non-motor, non-visual recruitment were modulated by training in the AAL-626 atlas. (**a**) Motor-visual integration and (**b**) non-motor, non-visual recruitment depended on the number of trials practiced. Solid diagonal lines indicate the best linear fit, and *r* values indicate Pearson correlation coefficients. Error bars indicate s.d. of the mean across participants. To quantify these observations, we again defined the training-dependent modulation of brain network diagnostics as $-r$, where r is the Pearson correlation coefficient between the logarithm of the number of trials practiced and the diagnostic value. Motor-visual integration showed significant training-dependent modulation ($r = -0.90$, $P = 5.54 \times 10^{-5}$), as did non-motor, non-visual recruitment ($r = -0.84$, $P = 4.05 \times 10^{-4}$).

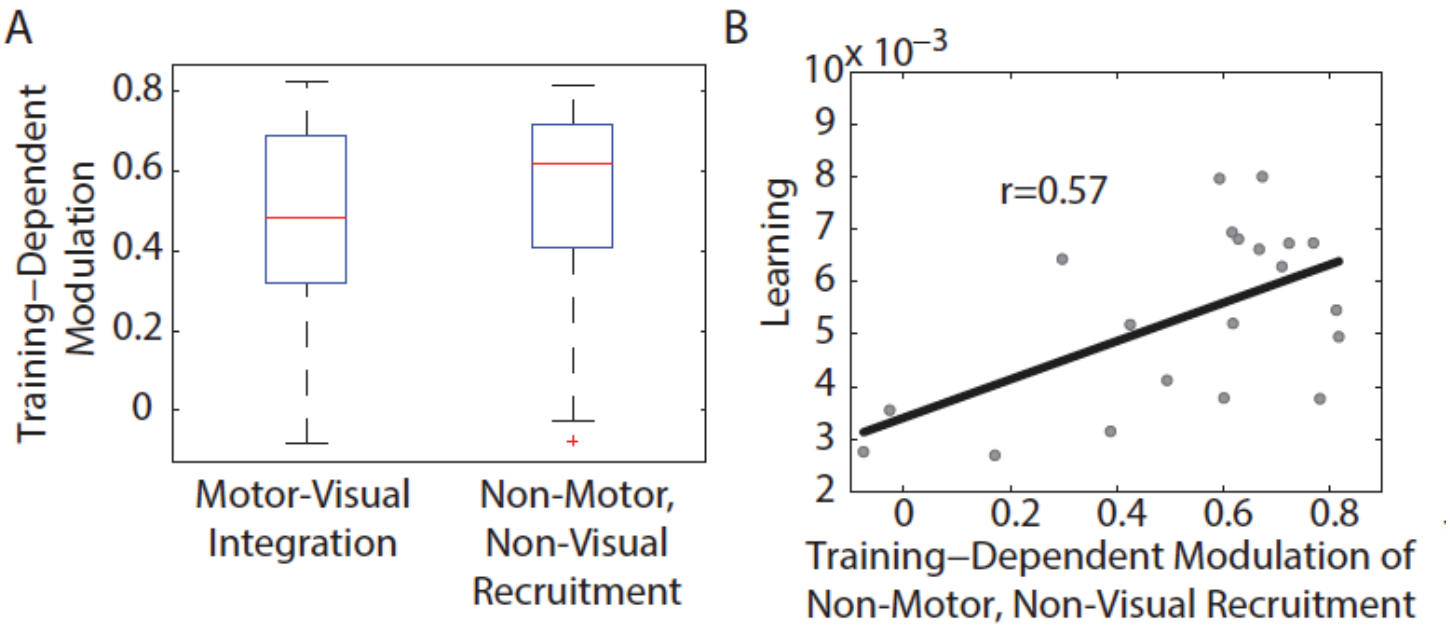

Supplementary Figure 12

Individual differences in brain network architecture map to task performance and task learning in finer-grained parcellation.

In the AAL-626 atlas, we observed a similar relationship between brain network architecture and individual differences in learning (compare to **Fig. 5***).* ***(a)*** *Box plots of task-dependent modulation (correlation between network diagnostic and number of trials practiced) for both motor-visual integration (left) and non-motor, non-visual recruitment (right).* ***(b)*** *Scatter plot of learning rate and training-dependent modulation of non-motor, non-visual recruitment (r = 0.57, P = 0.0062).*

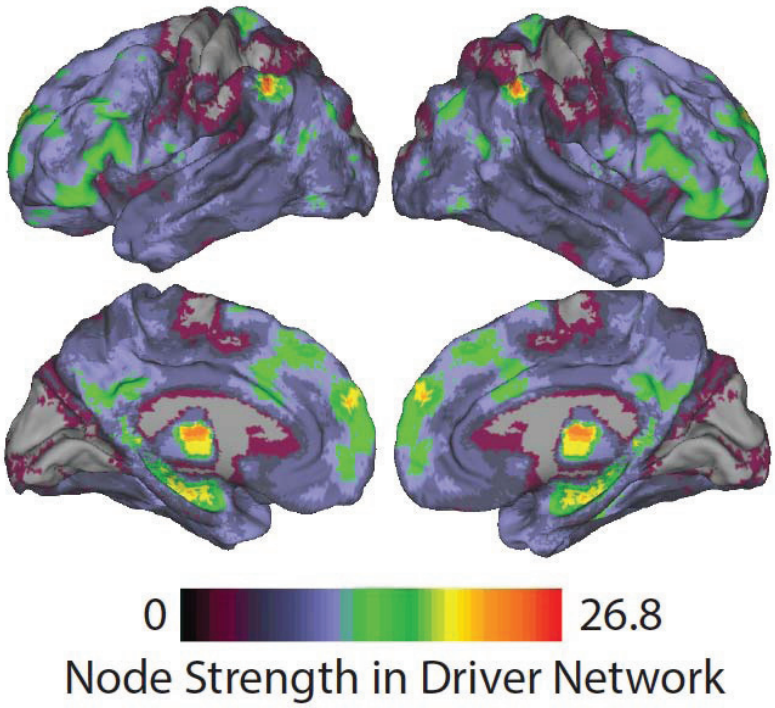

Supplementary Figure 13

The release of a fronto-cingulate control network in finer-grained parcellation predicts individual differences in learning.

In the AAL-626 atlas, we observed that the release of a fronto-cingulate control network predicted individual differences in learning, corroborating our results obtained with the Harvard-Oxford atlas. The 8,286 elements in the driver network are given by the statistically significant ($P < 0.05$, uncorrected) Pearson correlation coefficients between individual differences in training-induced modulation and individual differences in learning rate. The distribution of strength values over brain areas was highly skewed ($s = 1.30$)—significantly more so than would be expected in a random-network null model (non-parametric test, $P < 0.00000$). Here we show the strength of brain areas in this driver network, mapped onto the cortical surface using Caret software (http://brainvis.wustl.edu). The strength of area i is given by the sum of column i in the driver network. Warm colors indicate high strength in the driver network, and cool colors indicate low strength in the driver network. In addition to those regions observed in the 112-region template, here we also notice the high strength of the temporo-parietal junction, and the entorhinal cortex.

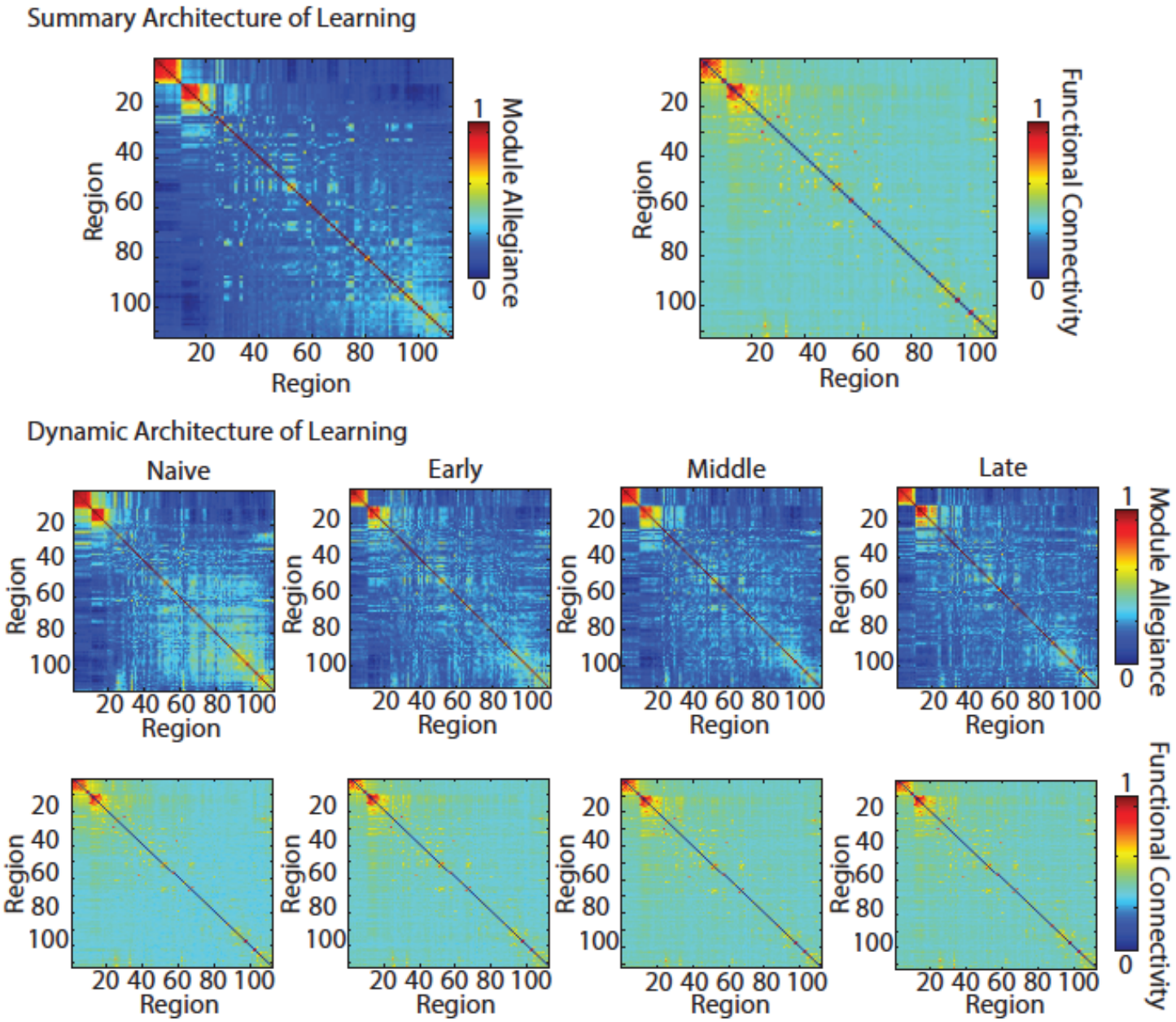

Supplementary Figure 14

Module-allegiance versus functional connectivity matrices.

When introducing any new method, it is important to ask whether similar results could have been uncovered using a simpler approach. Here we show that module-allegiance matrices provide a level of sensitivity to learning-related changes in brain network architecture that is not observed in functional connectivity matrices. We subdivide this exposition into discussions of (i) summary and dynamic architecture of learning (in this figure caption) and (ii) recruitment and integration modulated by training (in the **Supplementary Math Note**). In **Figure 2** we show the module-allegiance matrix $\boldsymbol{P}$, whose elements P_{ij} give the probability that area i and j are in the same community across all subjects, scanning sessions, sequence types, and trial blocks. At the top of this figure, we show the average functional connectivity matrix $\boldsymbol{W}$ for comparison. The elements W_{ij} give the wavelet coherence values averaged over all subjects, scanning sessions, sequence types, and trial blocks. Motor and visual areas are less delineated in the average functional connectivity matrix than in the module-allegiance matrix. In **Figure 3** we show the module-allegiance matrices for the naive, early, middle, and late learning sessions separately. For the naive module-allegiance matrix $\boldsymbol{P}_{\text{naive}}$, the elements P_{ij} give the probability that area i and j are in the same community over all subjects, sequence types, and trial blocks in the naive scanning session. Module-allegiance matrices for

the other three scanning sessions were constructed similarly. At the bottom of this figure, we show the average functional connectivity matrices for comparison. For the naive functional connectivity matrix $\boldsymbol{W}_{\mathbf{naive}}$, the elements W_{ij} give the wavelet coherence averaged over all subjects, sequence types, and trial blocks in the naive scanning session. Average functional connectivity matrices for the other three scanning sessions were constructed similarly. We observed that (i) motor and visual areas were less delineated, (ii) changes in motor-visual integration were less clear, and (iii) the coherent involvement of the non-motor, non-visual areas was less pronounced in the average functional connectivity matrices than in the module-allegiance matrices. We normalized the functional connectivity matrices in this figure by dividing by the mean for comparability of visualizations. In the **Supplementary Math Note**, we show that alternative estimates of recruitment and integration based on the functional connectivity matrix rather than the module-allegiance matrix did not provide sensitivity to learning-related changes in brain network architecture.

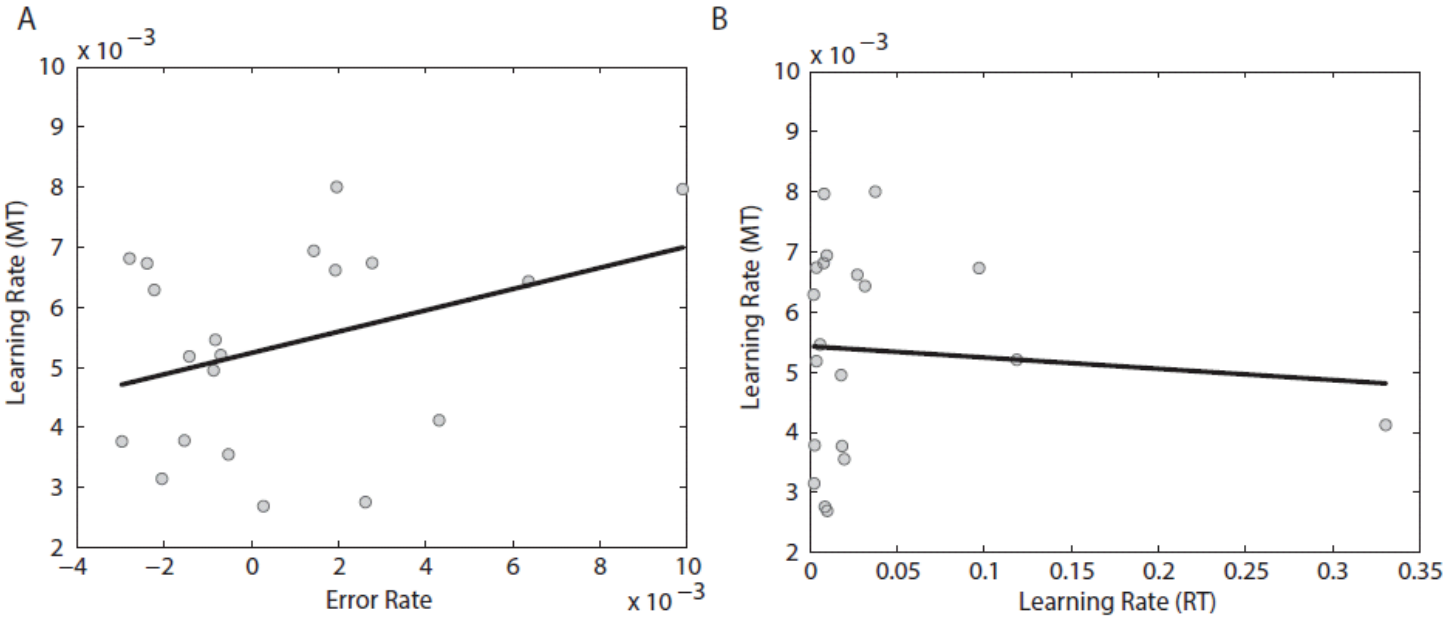

Supplementary Figure 15

Alternative quantifications of behavior.

Movement time is the canonical behavioral measure of motor-sequence learning. However, error rates and reaction times can in some experimental designs provide additional insights. Here we show that error rates and reaction-time rates were not correlated with (i) learning rate, (ii) training-dependent modulation of motor-visual integration, or (iii) training-dependent modulation of non-motor, non-visual recruitment. These results suggest that our findings relating learning rates to training-dependent changes in network reconfiguration are specific and do not relate more broadly to other behavioral characteristics such as error rates and reaction-time rates.

In this particular experiment, subjects were instructed to remain as accurate as possible, and therefore error rates are quite low in this data set. Nevertheless, errors did occur, and their number varied from subject to subject. To address the effects of errors, we performed an additional analysis to (i) estimate errors as a function of training, (ii) determine the relationship between error rate and movement time, and (iii) quantify the relationship between the training-dependent modulation of error rate and training-dependent modulation of motor-visual integration and non-motor, non-visual recruitment. To estimate errors as a function of training, we ordered all trials (including all six sequences) according to the amount of training. For each subject, we divided the number of trials into 45 equally sized bins (similar results were obtained for 15–120 bins) and calculated the error rate (e.g., percent correct) in each bin. Because subjects had an almost identical number of trials, the number of trials per bin was comparable across subjects. We fit the data of error rate versus trial bin using a first-degree polynomial with a single slope parameter (used to measure the training-dependent modulation of error rate) and constant. We next determined the relationship between the training-dependent modulation of error rate and the learning rate . We observed no significant relationship between these two variables: the Pearson correlation coefficient between and was r = 0.34, P = 0.13 (**a**; each data point indicates a single subject). This result indicates that individuals who are good learners do not show an increase or decrease in error rate over training in comparison to poor learners. This finding shows that our subjects were indeed learning the sequences: they moved much more quickly with training while remaining similarly accurate. Our data therefore do not support a simple speed-accuracy tradeoff. Finally, we determined the relationship between the training-dependent modulation of error rate and the training-dependent modulation of motor-visual integration and non-motor, non-visual recruitment. We observed no significant relationship between and training-dependent modulation of motor-visual integration (r = 0.04, P = 0.87) or non-motor, non-visual recruitment (r = 0.15, P = 0.52). This indicates that individuals who show greater training-dependent modulation of motor-visual integration and non-motor, non-visual recruitment do not tend to show an increase or decrease in error rates over training in comparison to individuals with less training-dependent modulation of motor-visual integration and non-motor, non-visual recruitment. Again, this finding is evidence for learning.

Reaction-time estimates have in some experimental scenarios provided additional behavioral insights into the mechanisms of learning. In our study, subjects were first presented with a symbolic cue indicating which of the six sequences to expect. After a variable delay, one of five spatial cues appeared, indicating the first element of the sequence. RT is the time between the appearance of the spatial cue and the first motor response. In the analysis of error rate, we binned error data of trial blocks to obtain continuous measurements from what was inherently binary data (e.g., error or no error). In contrast, reaction time is itself a continuous measure, and therefore we can treat it the same as movement time by performing a double exponential fit with robust outlier correction to home training session behavioral data. We next determined the relationship between the reaction-time rate $_{RT}$ and the learning rate . We observed no significant relationship between the two variables: $r = –0.08$ and $P = 0.73$ (**b**; each data point indicates a single subject). Because $_{RT}$ values appeared to be heavily skewed, we confirmed this lack of relationship using a Spearman rank correlation (= 0.09, $P = 0.70$). This result indicates that individuals who are good learners do not show a different reaction-time rate than poor learners. Finally, we determined the relationship between the reaction-time rate $_{RT}$ and the training-dependent modulation of motor-visual integration and non-motor, non-visual recruitment. We observed no significant relationship between $_{RT}$ and training-dependent modulation of motor-visual integration ($r = –0.17$, $P = 0.46$) or non-motor, non-visual recruitment ($r = –0.35$, $P = 0.13$). This result indicates that individuals who show greater training-dependent modulation of motor-visual integration and non-motor, non-visual recruitment do not tend to show unusually high or low reaction-time rates.

These results suggest that the findings reported in the article relating learning rates to training-dependent changes in network reconfiguration are specific and do not relate more broadly to other behavioral characteristics such as error rates and reaction-time rates.

Supplementary Math Note for Learning-Induced Autonomy of Sensorimotor Systems

Danielle S. Bassett[1,2,*], Muzhi Yang[1,3], Nicholas F. Wymbs[4], Scott T. Grafton[4]

[1]*Department of Bioengineering, University of Pennsylvania, Philadelphia, PA, 19104, USA*
[2]*Department of Electrical Engineering, University of Pennsylvania, Philadelphia, PA, 19104, USA*
[3]*Applied Mathematics and Computational Science Graduate Group, University of Pennsylvania, Philadelphia, PA, 19104, USA*
[4]*Department of Psychological and Brain Sciences and UCSB Brain Imaging Center, University of California, Santa Barbara, CA 93106, USA*

Nature Neuroscience: doi:10.1038/nn.3993

Contents

Nature Neuroscience: doi:10.1038/nn.3993

Supplementary Math Note

Dynamic Community Detection Community detection (Porter et al. (2009) "Communities in networks", *Not Amer Math Soc*, **56**, 1082–1097, 1164–1166; Fortunato (2010) "Community detection in graphs", *Phys Rep*, textbf486, 75–174) can be used to identify putative functional modules (i.e., sets of brain regions that exhibit similar trajectories through time). One such technique is based on the optimization of the modularity quality function (Newman & Girvan (2004) "Finding and evaluating community structure in networks", *Phys Rev E*, **69**, 026113; Newman (2006) "Modularity and community structure in networks", *Proc Natl Acad Sci USA*, **103**, 8577–8582; Newman (2006) "Finding community structure in networks using the eigenvectors of matrices", *Phys Rev E*, **74**, 036104). This allows one to identify groups that consist of nodes that have stronger connections among themselves than they do to nodes in other groups (Porter et al. (2009) "Communities in networks", *Not Amer Math Soc*, **56**, 1082–1097, 1164–1166). Recently, the modularity quality function has been generalized so that one can consider time-dependent or multiplex networks using *multilayer modularity* (Mucha et al. (2010) "Community structure in time-dependent, multiscale, and multiplex networks", *Science*, **328**, 876–878)

$$Q = \frac{1}{2\mu} \sum_{ijlr} \left\{ \left(A_{ijl} - \gamma_l M_{ijl} \right) \delta_{lr} + \delta_{ij} \omega_{jlr} \right\} \delta(g_{il}, g_{jr}) \,, \tag{1}$$

where the adjacency matrix of layer l has components A_{ijl}, the element M_{ijl} gives the components of the corresponding matrix for a null model, γ_l is the structural resolution parameter of layer l, the quantity g_{il} gives the community (i.e., "module") assignment of node i in layer l, the quantity g_{jr} gives the community assignment of node j in layer r, the parameter ω_{jlr} is the connection strength—i.e., "interlayer coupling parameter", which gives an element of a tensor ω that constitutes a set of *temporal resolution parameters* if one is using the adjacency tensor $\mathbf{A}$ to represent a time-dependent network—between node j in layer r and node j in layer l, the total edge weight in the network is $\mu = \frac{1}{2} \sum_{jr} \kappa_{jr}$, the strength of node j in layer l is $\kappa_{jl} = k_{jl} + c_{jl}$, the intra-layer strength of node j in layer l is k_{jl}, and the inter-layer strength of node j in layer l is $c_{jl} = \sum_r \omega_{jlr}$. We employ the Newman-Girvan null model within each layer by using

$$M_{ijl} = \frac{k_{il} k_{jl}}{2m_l} \,, \tag{2}$$

where $m_l = \frac{1}{2} \sum_{ij} A_{ijl}$ is the total edge weight in layer l. We let $\omega_{jlr} \equiv \omega =$ constant for neighboring layers (i.e., when $|l - r| = 1$) and $\omega_{jlr} = 0$ otherwise. We also let $\gamma_l = \gamma =$ constant. For simplicity and in line with previous work (Bassett et al. (2011) "Dynamic reconfiguration of human brain networks during learning", *Proc Natl Acad Sci USA*, **108**, 7641–7646; Bassett et al. (2013) "Task-based core-periphery structure of human brain dynamics", *PLoS Comp Biol*, **9**, e1003171), here we set $\omega = 1$ and $\gamma = 1$.

Description of Statistical Null Model for the Inference of Module Allegiance Values In the main manuscript, we describe a method for constructing the module allegiance matrix $\mathbf{P}$, whose

elements P_{ij} represent the probability that area i and j are in the same community over a set of partitions (e.g., subjects, trial blocks, scans, etc.). This module allegiance matrix is a normalized version of the nodal association matrix described in (Bassett, et al. (2013) "Robust detection of dynamic community structure in networks", *Chaos*, **23**, 1): $\mathbf{T}$ whose elements T_{ij} indicate the number of times that nodes i and j are in the same community. To determine which elements of $\mathbf{T}$ have probability values higher than expected, we construct a null-model association matrix $\mathbf{T}^{\mathrm{r}}$ based on random permutations of the original set of partitions.

To be concrete, let us examine the module allegiance matrices constructed for each scanning session. Here, each nodal association matrix $\mathbf{T}$ is computed over the set of partitions composed of subjects and trial blocks in a single scanning session (naive, early, middle, and late). To construct an associated null model for this structure, we perform the following steps as described in (Bassett, et al. (2013) "Robust detection of dynamic community structure in networks", *Chaos*, **23**, 1). First, for each of the C partitions, we reassign nodes uniformly at random to the n communities that are present in the selected partition. For every pair of nodes i and j, we let T^r_{ij} be the number of times these two nodes have been assigned to the same community in this permuted situation. The values T^r_{ij} then form a distribution for the expected number of times two nodes are assigned to the same partition. We observe that two nodes can be assigned to the same community a number of times out of the C partitions purely by chance: the average being 38.89 times out of every 100 partitions, or 38.89%. To be conservative, we remove such 'noise' from the original nodal association matrix $\mathbf{T}$ by setting any element T_{ij} whose value is less than the maximum entry of the random association matrix to 0. This yields the thresholded matrix $\mathbf{T}'$, which retains statistically significant relationships between nodes. We then transform $\mathbf{T}'$ to a probability matrix $\mathbf{P}'$, whose elements P_{ij} are either 0 (if the associated element in $\mathbf{T}'$ is 0) or the probability that area i and j are in the same community over the set of partitions (if the associated element in $\mathbf{T}'$ is nonzero). In Fig. 1, we show the thresholded $\mathbf{P}'$ matrices corresponding to the unthresholded $\mathbf{P}$ matrices visualized in the main manuscript. We observe that the four features described in the main text – (i) motor recruitment, (ii) visual recruitment, (iii) motor-visual integration, and (iv) non-motor, non-visual recruitment – are preserved following this statistical correction.

Recruitment and Integration Modulated by Training The definitions of module recruitment and integration provided in the main manuscript utilize the module allegiance matrix $\mathbf{P}$, whose elements P_{ij} give the probability that area i and j are in the same community. As stated in the main manuscript, we let $\mathcal{C} = \{C_1, \cdots, C_k\}$ be the partition of brain regions into groups. Then

$$I_{k_1,k_2} = \frac{\sum_{i \in C_{k_1}, j \in C_{k_2}} P_{ij}}{|C_{k_1}||C_{k_2}|} \tag{3}$$

is the interaction strength between group C_{k_1} and group C_{k_2}, where $|C_k|$ is the number of nodes in group C_k. We use this quantity to determine module recruitment and integration, depending on whether the two groups are identical ($k_1 = k_2$) or different ($k_1 \neq k_2$).

It is also possible to compute alternative estimates of recruitment and integration based on

Nature Neuroscience: doi:10.1038/nn.3993

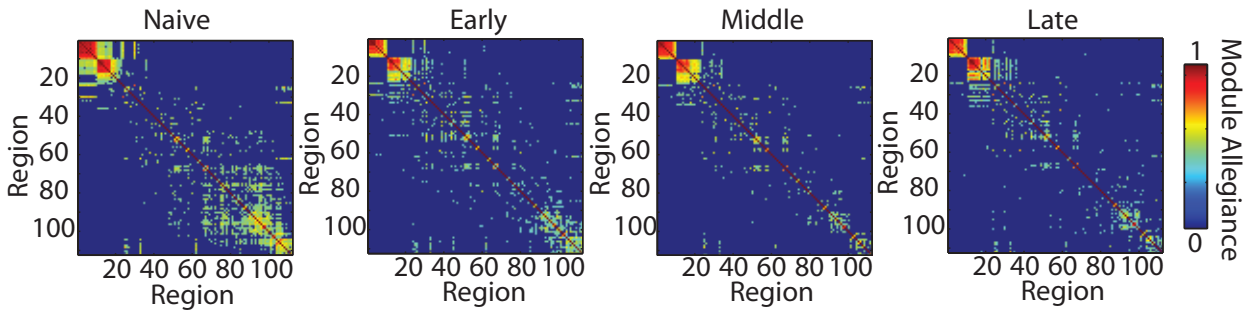

Figure 1: **Dynamic Brain Architecture Associated with Task Practice Confirmed After Statistical Correction of Module Allegiance Values** Here, the unthresholded module allegiance matrices given in the main manuscript are presented after the application of a statistical threshold on the module allegiance values. We observe that the four features described in the main text – (i) motor recruitment, (ii) visual recruitment, (iii) motor-visual integration, and (iv) non-motor, non-visual recruitment – are preserved following this statistical correction.

the functional connectivity matrix $\mathbf{W}$, whose elements W_{ij} give the wavelet coherence between the BOLD time series of area i and that of area j. It is very important to ask whether such a substitution provides equal or better sensitivity to learning-related changes in brain network architecture.

To address this question, we first note that the probability matrices $\mathbf{P}$ constructed to capture the dynamic architecture of learning collapse information across trial blocks. For comparability, we therefore averaged functional connectivity matrices across trial blocks to create mean functional connectivity matrices $\overline{\mathbf{W}}$ separately for each subject, training intensity (extensively, moderately, and minimally trained sequences) and duration (naive, early, middle, and late). We then replace P_{ij} with $\overline{W_{ij}}$, such that

$$I'_{k_1,k_2} = \frac{\sum_{i \in C_{k_1}, j \in C_{k_2}} \overline{W_{ij}}}{|C_{k_1}||C_{k_2}|} \tag{4}$$

is an alternative estimate of the interaction strength. In Fig. 2, we show the values of the four brain network diagnostics (motor, visual, and non-motor non-visual recruitment and motor-visual integration) computed using I' (Equation 4) rather than I (Equation 3). We observe that none of these diagnostics display training-dependent modulation consistent with the number of trials practiced. Instead, we tend to observe relatively independent effects of either training intensity (see Fig. 2A & D) or training duration (see Fig. 2B), or neither (see Fig. 2C).

Description of Statistical Null Model for the Skewness of the Driver Network The asymmetry of strength distributions in the driver indicates that some brain areas participate in many functional interactions that predict learning. Based on the field of mathematics known as *graph theory*, we can postulate that this level of skewness is unexpected in a purely random or noisy system. To test this hypothesis, we create an ensemble of 100,000 Erdős-Rényi graphs with the same number of nodes (90) and edges (180) as the driver network. We then distribute the strength values of the edges of the driver network uniformly at random over the edges of the Erdős-Rényi graph,

Nature Neuroscience: doi:10.1038/nn.3993

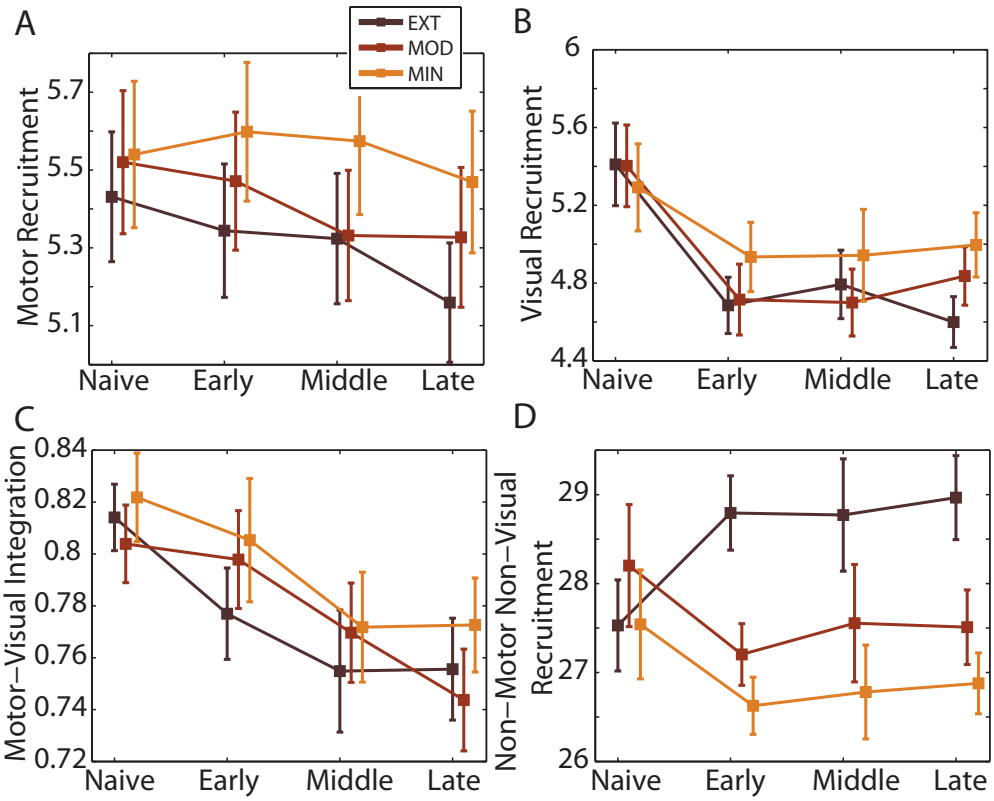

Figure 2: **Alternative Estimates of Recruitment and Integration Obtained from Functional Connectivity Matrices** *(A)* Motor, *(B)* visual, and *(C)* non-motor, non-visual recruitment and *(D)* motor-visual integration as a function of training intensity (extensively (maroon), moderately (red), and minimally (orange) trained sequences) and duration (naive, early, middle, and late). Error bars indicate standard deviation of the mean over participants.

and calculate the skewness of the strength distribution over network nodes. Using these values as a null distribution, we conclude that the observed value of skewness in the true driver network ($s = 1.89$) is significantly greater than that expected under the null hypothesis of random structure: $p = 0.00009$.

Description of Null Model for Effect of Region Size Recent studies have noted that brain-region size can affect estimates of hard-wired connectivity strength used in constructing structural connectomes (Hagmann et al. (2008) "Mapping the structural core of human cerebral cortex", *PLoS Biol*, **6**, e159; Bassett et al. (2011) "Conserved and variable architecture of human white matter connectivity", *NeuroImage*, **54**, 1262–1279). In prior work we demonstrated that region size does not have an appreciable effect on dynamic community structure in brain networks extracted during motor learning (Bassett et al. (2013) "Task-based core-periphery structure of human brain dynamics", *PLoS Comp Biol*, **9**, e1003171). However, it is nevertheless relevant to consider whether or not region size could be a driving effect of the observed organization in the module allegiance matrices.

Nature Neuroscience: doi:10.1038/nn.3993

To address this possibility, we asked whether the motor and visual modules are composed of unusually large or unusually small brain areas. We estimated the size of brain areas in terms of voxels (averaged over participants). We then calculated the average size of all regions in the motor module (*average size of motor region*), the average size of all regions in the visual module (*average size of visual region*), and the average size of all regions in the non-motor, non-visual set (*average size of non-motor non-visual region*). We then constructed a null distribution for each of these statistics by randomly reassigning region labels to the 3 groups (motor, visual, and non-motor non-visual) for a total of 1000 times. None of these groups contains significantly larger/smaller areas than expected under the null hypothesis: for the motor module $p = 0.93$/$p = 0.07$, visual module $p = 0.30$/$p = 0.70$, and non-motor non-visual set $p = 0.21$/$p = 0.79$. This suggests that region size is not driving the observed organization of the module allegiance matrix.

Nature Neuroscience: doi:10.1038/nn.3993